



# Approach for Numerical Modeling of Strain-Hardening Materials Using Double-Yield Model

Yihe Yu<sup>1,2</sup> · Liqiang Ma<sup>3</sup> · Dongsheng Zhang<sup>3</sup> · Faqiang Su<sup>1,4</sup>  · Guoying Wang<sup>1</sup>

Received: 23 November 2021 / Accepted: 7 April 2022 / Published online: 27 August 2022  
© The Author(s), under exclusive licence to Springer-Verlag GmbH Austria, part of Springer Nature 2022

## Abstract

The strain-hardening behavior of soils and rocks under compression is critical for evaluating the construction stability in geological and mining engineering. Numerical simulation is an effective approach and widely used in the stability analysis of constructions. To ensure the accuracy of the simulation results, it is necessary to select appropriate constitutive models and determine the correct model parameters. The double-yield model, built in FLAC<sup>3D</sup>, is often used to describe the strain-hardening behavior of geotechnical materials. On the assumption that there is only volume yielding in the material, a relationship between the cap pressure, plastic strain in the double-yield model, and the axial stress–strain in the compression test with axial loading and four lateral-face constraints was established. Then, the cap pressure and plastic strain could be calculated directly by a series of known axial stress–strain data. With this calculation method, the double-yield model parameters can be determined quickly and accurately. This method was derived based on the constitutive equation of the double-yield model and could quickly determine the model parameters by reverse calculation according to the expected results, so it was more efficient and credible than the more widely used trial-and-error method. Based on comparisons between the calculation and trial-and-error methods, some case studies also proved its efficiency and effectiveness. Moreover, there are no requirements for the source of known stress–strain data. Therefore, this method can be applied to the model parameter assignment based on the stress–strain data from experimental tests, theoretical analyses, empirical formulas, and other numerical simulations.

## Highlights

- A relationship between the double-yield model parameters and the axial stress-strain in a uniaxial loading test with lateral constraints was established.
- An approach for accurate numerical modeling of strain-hardening materials using a double-yield model was developed.
- Some contrastive analyses with similar studies were conducted to verify the accuracy and efficiency of the approach in this paper.

---

✉ Liqiang Ma  
ckma@cumt.edu.cn

✉ Faqiang Su  
sufq@hpu.edu.cn

<sup>1</sup> Henan Key Laboratory for Green and Efficient Mining and Comprehensive Utilization of Mineral Resources, Henan Polytechnic University, Jiaozuo 454003, Henan, China

<sup>2</sup> State Collaborative Innovation Center of Coal Work Safety and Clean-Efficiency Utilization, Henan Polytechnic University, Jiaozuo 454003, Henan, China

<sup>3</sup> School of Mines, China University of Mining and Technology, Xuzhou 221116, China

<sup>4</sup> State Key Laboratory of Coal Resources in Western China, Xi'an University of Science and Technology, Xi'an 710054, Shaanxi, China

**Keywords** Strain-hardening · Double-yield model · FLAC<sup>3D</sup> · Numerical simulation · Salamon model

## 1 Introduction

Soils and loose rocks are common geological and mining engineering materials, and they typically exhibit strain-hardening behavior. This mechanical behavior under compression should be considered for the stability of both surface and underground workings (Comodromos et al. 2018; Chen et al. 2019; Nematollahi and Dias 2018; Venda et al. 2017). For example, the stability of embankments and foundations on such soils may be affected by the strain-hardening behavior of soils (Venda et al. 2017). During the excavation of an underground space, the operation and maintenance of the space will depend on the soil hardening characteristics. In addition, the strain-hardening of caved rock and coal determines the distribution of coal mining pressure, and therefore, influences the support of the mining face and tunnel (Feng et al. 2018a; Li et al. 2018; Jiang et al. 2017; Gao et al. 2019). During backfill mining, some filling materials also exhibit strain-hardening properties when compressed, which may affect the filling effect (Yadav et al. 2020; Sahoo et al. 2020; Feng and Wang 2020; Wang et al. 2017).

Numerical simulation is a valuable and effective method for investigating the complicated deformation of soils and rocks. FLAC<sup>3D</sup>, one of the most widely used simulation software, establishes a nonlinear model called the double-yield model for analyzing strain-hardening materials. This double-yield model is a shear and volumetric hardening model that can reliably represent the loading–unloading response of soils (Itasca 2012). The numerical parameters of the double-yield model must be set correctly to accurately simulate the strain-hardening behavior of materials and to obtain satisfactory results. An acceptable approach involves determining the mechanical characteristics of materials in the laboratory, performing numerical simulations using relevant software, and adjusting the model parameters until the numerical results are consistent with the laboratory results. This approach is the so-called trial-and-error method, which is widely used in mining and geotechnical engineering (Gao et al. 2019; Li et al. 2019, 2017; Ataei et al. 2019).

However, at least two problems are encountered in the trial-and-error method. The first problem is the difficulty to juggle the accuracy and efficiency. In the double-yield model, the critical parameters influencing the strain-hardening behavior are the plastic strain and the corresponding cap pressure. The stress–strain curve of an ideal hardening material in the loading direction is a continuous curve. Multiple groups of plastic strains and the corresponding cap pressures need to be specified to fit the curve. These data form a two-dimensional polyline, controlling the

deformation of strain-hardening materials. The more data groups of plastic strain and cap pressure there are, the better the polyline fits the actual stress–strain curve. In the trial-and-error method, the number of the groups of plastic strain and cap pressure needs to be determined and each group should be tested repeatedly to be as close as possible to the actual stress–strain curve. Therefore, intensive effort is required to determine the appropriate numerical parameters and obtain ideal simulation results. The second problem is that it is challenging to assess complex heterogeneous materials, although they are heterogeneous in one direction. For example, for a longwall mining gob, the initial and final compaction degrees of the caved rock are different due to the different caving heights of the overlying strata, and the deformation characteristics under the overlying load are different. In this case, the double-yield model used to simulate different gob areas should be assigned different parameters, suggesting that it is difficult to apply the trial-and-error method to this situation.

In this study, the effects of double-yield model parameters on the stress–strain curve of materials under axial loads and four roller-constrained faces were analyzed. A corresponding relationship between the model parameters and the stress–strain curve was established. Based on this relationship, a calculation method for determining the model parameters was developed. The proposed method makes it easy and convenient to simulate the strain-hardening behavior of double-yield materials if the stress–strain data are known, regardless of the experimental tests, theoretical analyses, empirical formulas, and other numerical simulations. Thus, the proposed numerical method is credible and effective for solving complex strain-hardening problems in geotechnical engineering.

## 2 Double-Yield Model

### 2.1 Deformation Characteristics of Double-Yield Materials

For a plastic material, such as rock or soil, the material will reach the plastic stage from the elastic stage with increased loading. In the double-yield model, the yield criteria, which include the shear, tension, and volume yielding, determine whether the material enters the plastic stage. When the material is in the plastic state, the principal strain increments at any point on the loading path include the elastic and plastic parts.

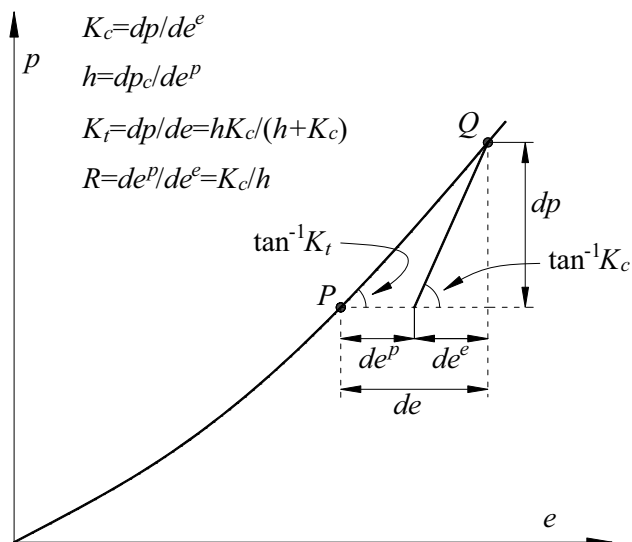


Fig. 1 Double-yield material in the isotropic consolidation test

$$\Delta \epsilon_i = \Delta \epsilon_i^e + \Delta \epsilon_i^p \quad (i = 1, 2, 3) \tag{1}$$

In Eq. (1), superscripts “e” and “p” denote the elastic and plastic parts, respectively. The plastic strains are decomposed into shear, tensile, and volumetric strains. In an isotropic compression test, only volumetric strain occurs, indicating that the plastic strain is equal to the plastic volumetric strain.

$$\Delta \epsilon_i^p = \Delta \epsilon_i^{pv} \tag{2}$$

In Eq. (2), the superscript “pv” refers to the plastic volumetric strain. On the strain-hardening curve (Fig. 1), Point P and its adjacent point, Point Q, are selected to define the elastic stiffness and plastic stiffness of the material at Point Q, as follows (Itasca 2012):

$$K_c = \frac{dp}{de^e} \tag{3}$$

$$h = \frac{dp_c}{de^p} \tag{4}$$

where  $K_c$  is the current tangential bulk modulus,  $p$  is the external average pressure,  $p_c$  is the cap pressure in the double-yield model, and  $h$  is the plastic modulus. In the volume yield stage,  $p = p_c$ . The observed tangent modulus at Point P of the main loading path can be expressed as follows:

$$K_t = \frac{hK_c}{h + K_c} \tag{5}$$

With an increasing pressure, the elastic stiffness and plastic stiffness of the material composed of small particles, such as rock or soil, may also increase because the

grains are compacted. In the double-yield model established in FLAC<sup>3D</sup>, the ratio of the elastic stiffness to the plastic stiffness is a constant factor,  $R$ , under general loading conditions (Itasca 2012).

$$\frac{K_c}{h} = \frac{de^p}{de^e} = R \tag{6}$$

The values of the initial bulk,  $K$ , and the shear modulus,  $G$ , provided by the user are adopted as the upper limits to  $K_c$  and  $G_c$ , respectively. It is assumed that the ratio  $K_c/G_c$  remains constant and is equal to  $K/G$ .

$$K_c = \min(K_c, K) \tag{7}$$

$$\frac{K_c}{G_c} = \frac{K}{G}$$

## 2.2 Volume Yield Function and Plastic Potential Function

In practice, materials are typically subjected to non-isotropic loading. In analyzing the effects of the double-yield model parameters on the strain-hardening behavior, it is assumed that only volume yielding occurs during compression. The yield surface (or “cap”) is a plane with three equal intercepts on the three coordinate axes in the principal stress space, where the volume yield function is expressed as follows:

$$f = \frac{1}{3}(\sigma_1 + \sigma_2 + \sigma_3) - p_c \tag{8}$$

where  $\sigma_1, \sigma_2,$  and  $\sigma_3$  are the three principal stresses. According to classical plasticity theory, a plastic potential surface exists in the plastic deformation field. The derivatives of the plastic potential surface provide the relative magnitudes of the plastic strain rates, which are expressed as follows:

$$\Delta \epsilon_i^p = \lambda \frac{\partial g}{\partial \sigma_i} \tag{9}$$

where  $\lambda$  is the plastic multiplier and  $g$  is the plastic potential function. Equation (9) is the plastic flow law, which defines the magnitude and direction of the plastic strain increment. The plastic flow law can be divided into associated and non-associated laws based on whether the plastic potential function is the same as the yield function. In FLAC<sup>3D</sup>, the volume yield obeys the associated plastic flow law; that is, the plastic potential function is the same as the yield function. Therefore, by combining Eqs. (8) and (9), the plastic strain increment and its components can be expressed as follows:

$$\Delta \varepsilon_i^p = \lambda \frac{\partial f}{\partial \sigma_i} = \frac{\lambda}{3} \quad (10)$$

$$\Delta \varepsilon^p = \sum_{i=1}^3 \Delta \varepsilon_i^p = \lambda.$$

In Eq. (1), the strain increments include the elastic and plastic parts. Equation (10) gives the plastic strain and its components; the elastic strain and its components can then be described as:

$$\Delta \varepsilon_i^e = \Delta \varepsilon_i - \Delta \varepsilon_i^p = \Delta \varepsilon_i - \frac{\Delta \varepsilon^p}{3} \quad (11)$$

$$\Delta \varepsilon^e = \sum_{i=1}^3 \Delta \varepsilon_i^e = \Delta \varepsilon - \Delta \varepsilon^p.$$

The incremental expression of Hooke's law in terms of the principal stress and strain has the following form (Itasca 2012):

$$\Delta \sigma_i = \left( K_c + \frac{4}{3} G_c \right) \Delta \varepsilon_i^e + \left( K_c - \frac{2}{3} G_c \right) (\Delta \varepsilon^e - \Delta \varepsilon_i^e) \quad (12)$$

$$= \left( K_c - \frac{2}{3} G_c \right) \Delta \varepsilon^e + 2 G_c \Delta \varepsilon_i^e,$$

where  $K_c$  and  $G_c$  are the current tangential bulk and shear moduli defined by Eqs. (3) and (7), respectively. Substituting Eq. (11) into Eq. (12), the three principle stresses and their sum can be obtained as follows:

$$\Delta \sigma_i = 2 G_c \Delta \varepsilon_i + \left( K_c - \frac{2}{3} G_c \right) \Delta \varepsilon - K_c \Delta \varepsilon^p \quad (13)$$

$$\sum_{i=1}^3 \Delta \sigma_i = 3 K_c (\Delta \varepsilon - \Delta \varepsilon^p).$$

In the volume yield stage, all points at the loading stress path satisfy the volume yield criterion expressed by Eq. (8). Hence, the cap pressure increment can be expressed as follows:

$$\Delta p_c = \frac{1}{3} (\Delta \sigma_1 + \Delta \sigma_2 + \Delta \sigma_3). \quad (14)$$

In the double-yield model, the cap pressure increment is related to the plastic strain increment (Itasca 2012). By substituting the second equation in Eq. (13) into Eq. (14), the plastic strain increment can be derived as follows:

$$\Delta \varepsilon^p = \Delta \varepsilon - \frac{\Delta p_c}{K_c}. \quad (15)$$

Equation (15) indicates that, during loading, the plastic volumetric strain increment is equal to the total strain minus the elastic parts.

## 2.3 Loading Path

For the mechanical boundary conditions of axial loads and four lateral-face roller constraints, the three principle stresses and strains can be expressed as follows:

$$\sigma_1 = \sigma_z \quad (16)$$

$$\sigma_2 = \sigma_3 = k_l \sigma_z$$

$$\varepsilon_1 = \varepsilon_z \quad (17)$$

$$\varepsilon_2 = \varepsilon_3 = 0,$$

where  $k_l$  is the lateral pressure coefficient. Equation (17) shows that the sum of the three principle strains, including the elastic and plastic parts, is equal to the axial strain. According to Eq. (6), the ratio of the plastic strain to the elastic strain is a constant  $R$ , and then the elastic and plastic strain can be expressed with the axial strain as follows:

$$\Delta \varepsilon^e = \frac{1}{R+1} \Delta \varepsilon_z \quad (18)$$

$$\Delta \varepsilon^p = \frac{R}{R+1} \Delta \varepsilon_z.$$

The following sections discuss the cap pressure. Substituting Eqs. (16) and (17) into Eq. (13) yields the following three principal stresses:

$$\Delta \sigma_1 = \left( K_c + \frac{4}{3} G_c \right) \Delta \varepsilon_z - K_c \Delta \varepsilon^p \quad (19)$$

$$\Delta \sigma_2 = \Delta \sigma_3 = \left( K_c - \frac{2}{3} G_c \right) \Delta \varepsilon_z - K_c \Delta \varepsilon^p.$$

According to Eqs. (7) and (18),  $K_c/G_c = K/G$  and  $\Delta \varepsilon^p = \Delta \varepsilon_z R/(R+1)$ , so Eq. (19) can be rewritten as follows:

$$\Delta \sigma_1 = \left( \frac{1}{R+1} + \frac{4G}{3K} \right) K_c \Delta \varepsilon_z \quad (20)$$

$$\Delta \sigma_2 = \Delta \sigma_3 = \left( \frac{1}{R+1} - \frac{2G}{3K} \right) K_c \Delta \varepsilon_z.$$

Equation (20) expresses the relationship between the three principal stresses and the axial strain of the double-yield model in the plastic deformation stage. According to Eq. (20), the lateral pressure coefficient  $k_l$  can be written as follows:

$$k_l = \frac{\Delta \sigma_3}{\Delta \sigma_1} = \frac{3K - 2G(R+1)}{3K + 4G(R+1)}. \quad (21)$$

In Eq. (21),  $K$ ,  $G$  and  $R$  are the predetermined parameters in the double-yield model. This means that the lateral pressure coefficient  $k_l$  is constant during compression. Therefore, the second and third principle stresses can be expressed as the product of the first principle stress and the lateral pressure coefficient. In the strain-hardening process, the three

principle stresses satisfy Eq. (14), so the following equation can be established.

$$\Delta p_c = \frac{1}{3}(\Delta\sigma_1 + k_l\Delta\sigma_1 + k_l\Delta\sigma_1) = \frac{1 + 2k_l}{3}\Delta\sigma_z. \tag{22}$$

In FLAC<sup>3D</sup>, the cap pressure and plastic volumetric strain are defined by the user to determine the hardening behavior of the material during compression. Equations (18) and (22) indicate a correspondence relationship between the plastic strain and axial strain, the cap pressure and axial stress under the boundary conditions of axial loads and four lateral-face roller constraints. If a series of axial stress–strain data are determined experimentally (or using other methods), then the cap pressure and plastic strain can be directly calculated using Eqs. (18) and (22).

### 2.4 Unloading Path

In the hardening curve under isotropic loading (Fig. 1), the unloading modulus is  $K_c$  if the material is unloaded at Point Q. Therefore, the volumetric properties  $R$  can be computed using Eq. (23).

$$R = \frac{K_c}{K_t} - 1. \tag{23}$$

For a uniaxial loading test with four lateral roller-constrained faces, the lateral stress is typically different from the axial stress. When Eq. (23) is directly used to determine  $R$ , it will introduce an error. As the difference between the loading modulus  $K_t$  and the unloading modulus  $K_c$  increases, this error will also increase. Thus, the volumetric properties  $R$  can be corrected using Eq. (24).

$$R = \frac{3}{1 + 2k_l} \left( \frac{K'_c}{K'_t} - 1 \right). \tag{24}$$

Substituting Eq. (21) into Eq. (24) solves the volumetric properties  $R$ .

$$R = \frac{(3K + 4G)(K'_c/K'_t - 1)}{3K - 4G(K'_c/K'_t - 1)}, \tag{25}$$

where  $K'_t$  is the axial loading modulus and  $K'_c$  is the axial unloading modulus.

### 2.5 Double-Yield Model Parameters

Several parameters must be defined in the double-yield model: the initial elastic bulk modulus  $K$  and shear modulus  $G$ , the yield strength parameters, that is, the tensile strength  $\sigma_t$ , cohesion  $c$ , and internal friction angle  $\varphi_f$ , the volumetric properties  $R$ , and the strain-hardening parameters, namely, the cap pressure  $p_c$  and plastic strain  $\varepsilon^p$ . These parameters

jointly control the compression hardening and unloading stress paths of double-yield materials. Based on the previous analysis, a calculation method is proposed to determine the parameters of the double-yield model, and the details are as follows:

(1) Initial elastic modulus.

The effects of the initial elastic bulk modulus  $K$  and shear modulus  $G$  on the mechanical behavior of materials result in the following three aspects. First, at any point in the loading path, the ratio of the current elastic bulk modulus to the shear modulus is equal to the ratio of the initial bulk modulus to the shear modulus, as expressed by Eq. (7). Second, the initial moduli  $K$  and  $G$  and the volumetric properties  $R$  influence the lateral pressure coefficient, as expressed by Eq. (21), which affects the relationship between the axial stress and cap pressure, as expressed by Eq. (22). Finally, the current elastic stiffness  $K_c$  cannot exceed the initial modulus  $K$ . When the ratios of the initial bulk modulus to the shear modulus are determined, their values do not affect the strain-hardening behavior of the material during compression. Therefore, the initial bulk and shear modulus values should be as high as possible to ensure that they consistently exceed the current elastic stiffness at any point in the loading path. Another noteworthy point is that the lateral pressure coefficient, determined by the initial elastic modulus  $K$ , the shear modulus  $G$  and the volumetric properties  $R$ , should range between zero and one.

(2) Yield strength parameters.

Yield strength parameters, such as the tensile strength  $\sigma_t$ , cohesion  $c$ , and internal friction angle  $\varphi_f$ , are the criteria for tensile and shear plastic yielding. The higher the values of the yield strength parameters are, the more difficult it is for the material to reach the corresponding yield stage. Here, it is assumed that the material only enters the volume yield stage during compression. Therefore, the tensile strength, cohesion, and internal friction angle should be as large as possible to ensure that the plastic deformation of the double-yield material does not include tensile and shear parts.

(3) Volumetric properties.

The volumetric properties  $R$  is used to control the slope of a stress–strain curve during unloading. When the unloading stress path is known and the initial bulk modulus and shear modulus have been determined by the user, the volumetric properties  $R$  can be calculated using Eq. (25).

(4) Cap pressure and plastic strain.

During the loading process, the tangent modulus of the stress–strain curve changes constantly, and the slope of each point on the cap pressure–plastic strain curve is different. For the convenience of calculation, the curve is approximately expressed as a polyline composed of  $n$  segments in FLAC<sup>3D</sup>, and all endpoints of the polyline should be on the cap pressure–plastic strain curve. A given stress–strain curve can also be regarded as an approximate polyline, in which

each endpoint corresponds to a set of axial stress and strain data. Thus, a series of corresponding cap pressure and plastic strain data can be calculated using Eqs. (18) and (22).

### 3 Case Analysis

#### 3.1 Soil Oedometer Test

In geotechnical engineering, the hardening characteristics of soil consolidation and compression must be considered for the stability of surface and underground workings. A comparison between the results of an oedometer test and a corresponding numerical simulation with a double-yield model has been presented in Comodromos et al. (2013), which is used as a case for the soil strain-hardening analysis in this section. Then, the double-yield model parameters were determined based on the experimental data obtained from the case using the calculation method. New numerical simulations were then performed and compared with the simulation results of the case (Fig. 2). The experimental and reconstituted curve data determined from the soil consolidation test in the case are listed in Table 1.

The unloading path of the double-yield model in FLAC<sup>3D</sup> is a straight line, and the unloading modulus is the current elastic stiffness  $K_c$  at the unloading starting point. However, there are two points in the unloading path for the oedometer test (in addition to the starting point), which can determine two unloading paths. It was assumed that the two unloading paths belonged to the oedometer test curve and reconstituted curve, and two groups of model parameters were determined (Tables 2 and 3).

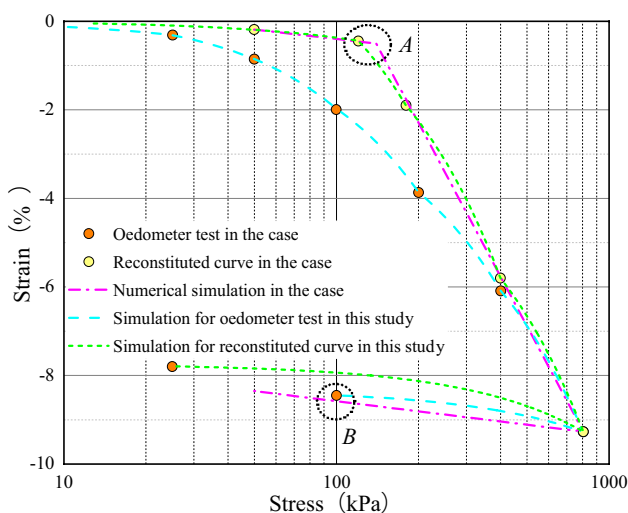


**Fig. 2** Comparison of the numerical results between Comodromos et al. (2013) and this study

**Table 1** Data for the oedometer test and the reconstituted curve from the case

Oedometer test		Reconstituted curve	
$\varepsilon_1$	$\sigma_1$ (Pa)	$\varepsilon_1$	$\sigma_1$ (Pa)
0	0	0	0
0.0031	25,055.4	0.0019	49,927.9
0.0085	49,951.2	0.0045	120,323.4
0.0199	99,751.6	0.019	180,021.4
0.0387	200,239.1	0.058	399,414.1
0.0609	400,732.7	0.0927	804,922.6
0.0927	804,922.6	0.078	24,969.4
0.0845	99,975.1	/	/

The numerical results for the parameters in Tables 2 and 3 are presented in Fig. 2. Although the numerical simulation curve provided in the case was consistent with the experimental data, deviations between the two results were observed in areas A and B. However, the numerical curve for the oedometer test and the reconstituted curve plotted in this study passed through all the original data points, and the accuracy was satisfactory.

#### 3.2 Gob Materials in Longwall Mining

In longwall coal mining, the caved rock in the gob is a typical hardening material. After excavating the coal seam, the overlying strata break and collapse, piling up in the gob, and numerous cavities are formed in the loose body of the caved rock (Zhang et al. 2016, 2014). With compaction of the caved rock, the internal cavities shrink, improving the deformation resistance capacity of the caved rock, which is the so-called strain hardening.

Salamon (1990) established a theoretical model to describe the mechanical behavior of gob materials under compression. Pappas and Mark (1993) conducted compression tests in a laboratory and proved that the Salamon model could be applied to gob materials. In their study, the caved rock was axially loaded into a cylindrical chamber to simulate the gob materials with the surrounding coal constrained and the overlying strata loaded. The experimental results showed that the axial stress and axial strain of the gob materials satisfy the following relationship:

$$\sigma_z = \frac{E_0 \varepsilon_z}{1 - \varepsilon_z / \varepsilon_m}, \quad (26)$$

where  $\sigma_z$  is the axial stress,  $E_0$  is the initial tangent modulus,  $\varepsilon_z$  is the axial strain, and  $\varepsilon_m$  is the maximum axial strain.

The double-yield model parameters, particularly the cap pressure and plastic strain, must be set correctly to ensure

**Table 2** Parameters of the double-yield model

	$K$ (GPa)	$G$ (GPa)	$K_t$ (MPa)	$K_c$ (MPa)	$R$	$k_l$
Oedometer test	2	0.1	12.7104	85.9692	10.0279	0.3645
Reconstituted curve	2	0.2	11.6962	52.9896	7.5599	0.2005

**Table 3** Plastic strain and cap pressure calculated from Table 1

Oedometer test		Reconstituted curve	
$\epsilon^p$	$p_c$ (Pa)	$\epsilon^p$	$p_c$ (Pa)
0	0	0	0
0.0028	14,392.2194	0.0017	23,316.4123
0.0077	28,813.0533	0.0039	56,191.2278
0.0179	57,588.5162	0.0168	84,070.2931
0.0352	115,646.5802	0.0512	186,527.0487
0.0554	231,013.0968	0.0819	375,900.1924
0.0843	462,629.1598	/	/

**Table 4** Axial stress and strain of the Salamon model

$\epsilon_z$	$\sigma_z$ (MPa)	$\epsilon_z$	$\sigma_z$ (MPa)	$\epsilon_z$	$\sigma_z$ (MPa)
0	0	0.09	4.85	0.18	18.90
0.01	0.38	0.10	5.70	0.19	22.30
0.02	0.78	0.11	6.65	0.20	26.60
0.03	1.22	0.12	7.72	0.21	32.22
0.04	1.70	0.13	8.94	0.22	39.90
0.05	2.22	0.14	10.34	0.23	50.98
0.06	2.78	0.15	11.97	0.24	68.39
0.07	3.41	0.16	13.88	/	/
0.08	4.09	0.17	16.15	/	/

that the deformation of the gob materials in the numerical model is consistent with Eq. (26). The trial-and-error method is often used to solve this problem (Gao et al. 2019; Yadav et al. 2020; Sahoo et al. 2020; Feng and Wang 2020; Li et al. 2019, 2015; Wang et al. 2016). For example, in Gao et al. (2019), the Salamon model parameters based on the mechanical properties of coal and rock in a mine were provided ( $E_0 = 36.27$  MPa;  $\epsilon_m = 0.275$ ), and the corresponding double-yield model parameters are obtained using the trial-and-error method. In this section, data on the Salamon model in Gao et al. (2019) were used to determine the double-yield model parameters by the calculation method, and the numerical results were compared with those presented in Gao et al. (2019) as a contrastive analysis.

First, a series of axial strain data of the gob materials under compression were determined, and the corresponding axial stress data were calculated using Eq. (26). The values are listed in Table 4.

As described in Sect. 2.5, the initial elastic modulus and yield strength parameters were set to be as high as possible.

**Table 5** Double-yield model parameters

$K$ (GPa)	$G$ (GPa)	$\sigma_t$ (GPa)	$c$ (GPa)	$\phi_f$ (°)	$R$
100	37.5	1	1	30	3

**Table 6** Plastic strain and cap pressure calculated from Table 4

$\epsilon^p$	$p_c$ (MPa)	$\epsilon^p$	$p_c$ (MPa)	$\epsilon^p$	$p_c$ (MPa)
0	0	0.0675	1.6174	0.1350	6.2995
0.0075	0.1255	0.0750	1.8999	0.1425	7.4318
0.0150	0.2608	0.0825	2.2165	0.1500	8.8660
0.0225	0.4071	0.0900	2.5740	0.1575	10.7415
0.0300	0.5659	0.0975	2.9808	0.1650	13.2990
0.0375	0.7388	0.1050	3.4479	0.1725	16.9932
0.0450	0.9278	0.1125	3.9897	0.1800	22.7983
0.0525	1.1353	0.1200	4.6257	/	/
0.0600	1.3640	0.1275	5.3829	/	/

The volumetric properties  $R$  influences the lateral pressure coefficient during loading and the slope of the stress–strain curve in the unloading path. In longwall mining, there is no unloading stage, and the caved rock in the gob typically does not induce lateral forces on the surrounding coal and rock. Therefore, the lateral pressure coefficient was assumed to be zero. As the values of  $K$  and  $G$  were known,  $R$  was computed using Eq. (21). The plastic strain and cap pressure were then calculated using Eqs. (18) and (22). All parameters of the double-yield model are listed in Tables 5 and 6.

Similar to Gao et al. (2019), a numerical cube model with a size of  $1\text{ m} \times 1\text{ m} \times 1\text{ m}$  was established in FLAC<sup>3D</sup>. The vertical planes and the bottom plane were roller-constrained, and a constant velocity of  $10^{-5}$  m/s was applied to the top plane of the model. With the double-yield model parameters provided in the previous sections, the axial stress–strain curve in the numerical simulations was plotted (Fig. 3).

Although Gao et al. (2019) stated that the numerical results for the parameters obtained using the trial-and-error method are in good agreement with the theoretical calculation results of the Salamon model, differences between both curves were observed. However, the simulation curve with the parameters provided in this study mostly overlaps with the theoretical curve. In addition, the horizontal stress curve shows that the lateral pressure coefficient is zero, as expected.

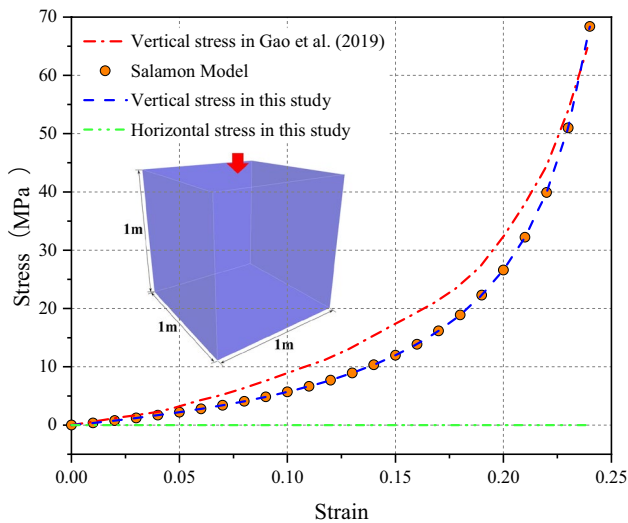


**Fig. 3** Comparison of the stress–strain curves between the theoretical and numerical simulations

Other numerical simulations were performed to further verify the accuracy and efficiency of the proposed parameter calculation method. In these numerical simulations, the double-yield model parameters were obtained using the calculation method, and the numerical results were compared with some similar research cases where the model parameters were determined using the trial-and-error method (Li et al. 2018; Jiang et al. 2017; Shen et al. 2018; Feng et al. 2018b). The plastic strain and cap pressure were calculated for each research case (Table 7), whereas the other parameters were

the same as those in the former case analysis in Gao et al. (2019). Although the model parameters provided in this study and these similar research cases are entirely different, the numerical results are similar (Fig. 4).

It appears that the trial-and-error method yielded satisfactory accuracy, but for different studies, the differences between the simulation and theoretical results were not the same. These differences suggest that the accuracy of the trial-and-error method may depend on the numerical simulation experience of the researchers. However, for these numerical models whose parameters were determined using the calculation method, the simulation results are completely consistent with the theoretical results. Hence, the gob materials can be accurately simulated without human errors.

## 4 Discussion

In the introduction of the double-yield model in the official manual for FLAC<sup>3D</sup>, an isotropic compression test is recommended, because it is best to determine the parameters related to a particular mode of failure from a test that only involves that particular failure mode. Therefore, a crucial assumption was made in developing this method; that is, only volume yield occurs during compression, while tensile and shear plastic yields do not occur. With this assumption, the failure mechanisms and stress regimes of materials are simple and clear. When the materials are axially loaded and laterally constrained, the axial stress increases, as does the

**Table 7** Plastic strain and cap pressure for similar research cases

Case 1 from Li et al. (2018)		Case 2 from Jiang et al. (2017)		Case 3 from Shen et al. (2018)		Case 4 from Feng et al. (2018b)	
$\epsilon^p$	$p_c$ (MPa)	$\epsilon^p$	$p_c$ (MPa)	$\epsilon^p$	$p_c$ (MPa)	$\epsilon^p$	$p_c$ (MPa)
0	0	0	0	0	0	0	0
0.0113	0.1036	0.0150	0.1436	0.0075	0.0711	0.0105	0.0362
0.0225	0.2217	0.0300	0.3067	0.0150	0.1501	0.0210	0.0777
0.0338	0.3573	0.0450	0.4936	0.0225	0.2383	0.0315	0.1258
0.0450	0.5148	0.0600	0.7101	0.0300	0.3376	0.0420	0.1823
0.0563	0.6998	0.0750	0.9635	0.0375	0.4502	0.0525	0.2493
0.0675	0.9205	0.0900	1.2643	0.0450	0.5788	0.0630	0.3304
0.0788	1.1880	0.1050	1.6273	0.0525	0.7272	0.0735	0.4303
0.0900	1.5191	0.1200	2.0738	0.0600	0.9003	0.0840	0.5565
0.1013	1.9395	0.1350	2.6363	0.0675	1.1049	0.0945	0.7210
0.1125	2.4911	0.1500	3.3671	0.0750	1.3504	0.1050	0.9443
0.1238	3.2465	0.1650	4.3547	0.0825	1.6504	0.1155	1.2647
0.1350	4.3442	0.1800	5.7635	0.0900	2.0254	0.1260	1.7634
0.1463	6.0855	0.1950	7.9358	0.0975	2.5075	0.1365	2.6462
0.1575	9.2703	0.2100	11.7229	0.1050	3.1503	0.1470	4.6357
0.1688	16.9651	0.2250	19.9914	0.1125	4.0501	0.1575	13.3037
0.1763	33.5612	/	/	0.1200	5.3995	/	/



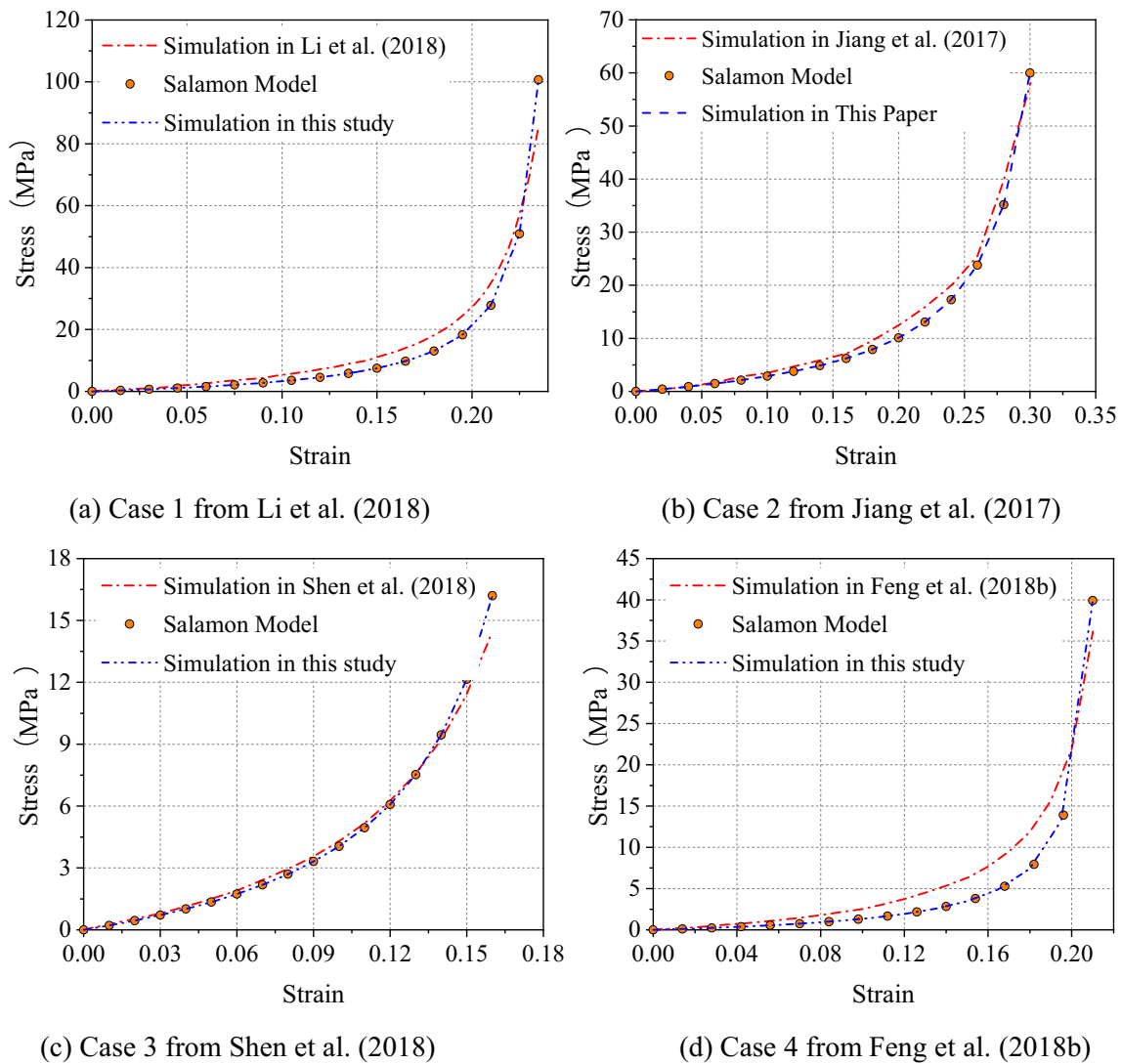


Fig. 4 Comparison of the numerical results between this study and the 4 cases

lateral stress, and the ratio of the axial stresses and lateral stresses is a constant, called the lateral pressure coefficient. Because the cap pressure in the double-yield model defined by the user increases from zero, volume yield deformation will occur at the beginning of the loading and continue throughout the entire loading process. This means that the sum of the three principle stresses, which are the axial stress and two identical lateral stresses, always equals triple the cap pressure, as shown in Eq. (14). For the strains under axial loads and the four lateral-face roller constraints, the sum of the three principle strains equals the axial strain, which includes the elastic and plastic parts. Considering that the ratio of the plastic strain to elastic strain is a constant  $R$ , the relationship between elastic strain, plastic strain and axial strain can be obtained, as shown in Eq. (18).

This assumption that only a volume yield occurs during compression appears to be unreasonable, but is acceptable in most cases. For example, the research focuses on the stress-strain relationship during loading and unloading, and the failure mechanisms of the material are not of great importance. The former is discussed in Comodromos et al. (2013), which provides the first example of a case study. In their study, the soil was modeled as a double-yield material to emphasize the significant effect and the need for settlement predictions for adjacent buildings. Therefore, provided that the compression and rebound of the soil in the numerical simulations are consistent with those of oedometer tests, it is unnecessary to focus on the plastic state of the soil. The latter can be found in the numerical simulations of the gob. When the double-yield model is used to describe the compaction deformation process of a caved rock in a gob, the

most significant problem is whether the vertical stress–strain curve satisfies expectations. The plastic state of gob materials, which are loose bodies of caved rocks, appears to lack any practical significance. In some similar studies, the cohesion in the numerical model obtained by different researchers using the trial-and-error method ranged from 0.01 to 1.7 MPa, whereas the internal friction angles ranged from 3° to 42°. For the initial bulk and shear moduli, the difference was up to three orders of magnitude (Feng et al. 2018a; Li et al. 2018; Jiang et al. 2017; Gao et al. 2019; Feng and Wang 2020; Ataei et al. 2019; Shen et al. 2018; Zhang et al. 2020). To some extent, this phenomenon suggests that these researchers did not focus on other parameters of gob materials except the vertical stress–strain characteristics, indicating that the calculation method proposed in this study may be an ideal approach for them.

## 5 Conclusions

In this study, a calculation method for determining the numerical parameters of the double-yield model was developed based on known stress–strain data. This method is only applicable to the loading conditions of axial loading and the four lateral roller-constrained faces. With this method, the mechanical behavior of the numerical model under compression could be completely consistent with the provided stress–strain data. In this method, the incremental expression of Hooke's law, in which the plastic strain is used to represent the principal stress, was deduced based on the constant ratio relationship between the elastic and plastic strains at any point in the hardening curve. Next, the relationship between the loading stress and the plastic volumetric strain was established based on the mechanical boundary conditions of axial loading and the four lateral roller-constrained faces. Thus, each group of cap pressure and plastic strain could be inversely calculated according to the corresponding group of axial stress and strain. There are no requirements for the source of known stress–strain data, indicating that the method can be applied to parameter determination based on the stress–strain data obtained from experimental tests, theoretical analyses, empirical formulas, and other numerical simulations.

According to this method, among these parameters of the double-yield model, the tensile strength, cohesion, and internal friction angle should be as large as possible to ensure that tensile or shear yielding of the material does not occur during compression. As the upper limit of the tangent modulus of the strain-hardening curve during compression, the initial bulk and shear modulus values should also be high to prevent errors. The volumetric properties  $R$  can be determined based on the slope of the stress–strain curve during volumetric unloading (if there is an unloading process). The

lateral pressure coefficient (ranging between zero and one) is influenced by the initial bulk modulus, shear modulus, and volumetric properties, which in turn is a constraint on the value range of these three parameters.

**Acknowledgements** This study was funded by the research fund of Henan Key Laboratory for Green and Efficient Mining & Comprehensive Utilization of Mineral Resources (KCF202006), the Doctor Foundation of Henan Polytechnic University (760207/029), National Natural Science Foundation of China (52104128), Key R & D and promotion projects in Henan Province (212102310010), Key Laboratory of Western Mine Exploitation and Hazard Prevention, Ministry of Education (SKLCKRF1902), Henan Province Key Scientific Research Project Plan for Colleges and Universities (22B440003).

## Declarations

**Conflict of interest** The authors declare that they have no conflict of interest.

## References

- Ataei M, Darvishi A, Rafiee R (2019) Investigating the effect of simultaneous extraction of two longwall panels on a maingate gateroad stability using numerical modeling. *Int J Rock Mech Mining Sci* 126
- Chen L, Qiao L, Li Q (2019) Study on dynamic compaction characteristics of gravelly soils with crushing effect. *Soil Dyn Earthq Eng* 120:158–169
- Comodromos EM, Papadopoulou MC, Konstantinidis GK (2013) Effects from diaphragm wall installation to surrounding soil and adjacent buildings. *Comput Geotech* 53:106–121
- Comodromos EM, Papadopoulou MC, Georgiadis K (2018) Design procedure for the modelling of jet-grout column slabs supporting deep excavations. *Comput Geotech* 100:110–121
- Feng GR, Wang PF, Chugh YP (2018a) Stability of gate roads next to an irregular yield pillar a case study. *Rock Mech Rock Eng* 52:2741–2760
- Feng GR, Wang PF, Yoginder PC (2018b) A new gob-side entry layout for longwall top coal caving. *Energies* 11:1292
- Feng GR, Wang PF (2020) Stress environment of entry driven along gob-side through numerical simulation incorporating the angle of break. *Int J Min Sci Technol* 30:189–196
- Gao YB, Wang YJ, Yang J, Zhang XY, He MC (2019) Meso- and macroeffects of roof split blasting on the stability of gateroad surroundings in an innovative nonpillar mining method. *Tunn Undergr Space Technol* 90:99–118
- Itasca (2012) *FLAC<sup>3D</sup> Fast Lagrangian analysis of continua User's and theory manuals*. Minneapolis Itasca Consulting Group
- Li B, Liang YP, Zhang L, Zou QL (2019) Experimental investigation on compaction characteristics and permeability evolution of broken coal. *Int J Rock Mech Min Sci* 118:63–76
- Li M, Zhang JX, Huang YL, Zhou N (2017) Effects of particle size of crushed gangue backfill materials on surface subsidence and its application under buildings. *Environmental Earth Sciences* 76:603
- Li WF, Bai JB, Peng S, Wang XY, Xu Y (2015) Numerical modeling for yield pillar design a case study. *Rock Mech Rock Eng* 48:305–318
- Li ZL, He XQ, Dou LM, Song DZ, Wang GF (2018) Numerical investigation of load shedding and rockburst reduction effects of top-coal caving mining in thick coal seams. *Int J Rock Mech Min Sci* 110:266–278

- Nematollahi M, Dias D (2018) Three-dimensional numerical simulation of pile-twin tunnels interaction—Case of the Shiraz subway line. *Tunn Undergr Space Technol* 86:75–88
- Pappas DM, Mark C (1993) Behavior of simulated longwall gob material
- Sahoo S, Behera B, Yadav A, Singh G, Sharma S (2020) Plane-Strain Modeling of Progressive Goaf Compaction in a Depillaring Working. *Journal of the Institution of Engineers Series D* 101:233–245
- Salamon M (1990) Mechanism of caving in longwall coal mining Rock mechanics contributions and challenges. *Proceedings of the 31st US symposium, Golden, Colorado*:161–168
- Jiang LS, Zhang PP, Chen LJ, Hao Z, Sainoki A, Mitri HS, Wang QB (2017) Numerical approach for goaf-side entry layout and yield pillar design in fractured ground conditions. *Rock Mech Rock Eng* 50:3049–3071
- Shen WL, Xiao TQ, Wang M, Bai JB, Wang XY (2018) Numerical modeling of entry position design A field case. *Int J Min Sci Technol* 28:985–990
- Venda PJ, Correia AAS, Lemos LJJ (2017) Numerical modelling of the effect of curing time on the creep behaviour of a chemically stabilised soft soil. *Comput Geotech* 91:117–130
- Wang J, Jiang JQ, Li GB, Hu H (2016) Exploration and numerical analysis of failure characteristic of coal pillar under great mining height longwall influence. *Geotech Geol Eng* 34:689–702
- Wang JC, Wang ZH, Yang SL (2017) A coupled macro- and meso-mechanical model for heterogeneous coal. *Int J Rock Mech Min Sci* 94:64–81
- Yadav A, Behera B, Sahoo SK, Singh GSP, Sharma S (2020) An Approach for Numerical Modeling of Gob Compaction Process in Longwall Mining. *Mining Metallurgy & Exploration* 37:631–649
- Zhang C, Bai QS, Chen YH (2020) Using stress path-dependent permeability law to evaluate permeability enhancement and coalbed methane flow in protected coal seam a case study. *Geomech Geophys Geo-Energy Geo-Resour* 6:1–25
- Zhang HZ, Deng KZ, Gu W (2016) Distribution law of the old goaf residual cavity and void. *J Min Safe Eng* 33:893–897
- Zhang N, Han CL, Kan JG, Zheng XG (2014) Theory and practice of surrounding rock control for pillarless gob-side entry retaining. *J Chin Coal Soc* 39:1635–1641

**Publisher's Note** Springer Nature remains neutral with regard to jurisdictional claims in published maps and institutional affiliations.